PERGAMON

International Journal of Heat and Mass Transfer 46 (2003) 535–550

International Journal of HEAT and MASS TRANSFER

www.elsevier.com/locate/ijhmt

Experimental investigation of the transient impact fluid dynamics and solidification of a molten microdroplet pile-up

S. Haferl, D. Poulikakos *

Laboratory of Thermodynamics in Emerging Technologies, Institute of Energy Technology, Swiss Federal Institute of Technology, 8092 Zurich, Switzerland

Received 9 October 2001; received in revised form 18 June 2002

Abstract

This paper presents an original systematic experimental investigation of the transient transport phenomena occurring during the pile-up of molten, picoliter-size liquid metal droplets. The prevailing physical mechanisms of the pile up process are identified and quantified experimentally. In terms of relevant dimensionless groups the following ranges are covered: $Re = 281–453$, $We = 2.39–5.99$, $Ste = 0.187–0.895$. This corresponds to molten solder droplets impinging at velocities ranging between 1.12 and 1.74 m/s having an average diameter of 78 μm. The impact fluid dynamics, cooling and subsequent solidification of the second (top) droplet in the pile-up is strongly influenced by the geometry of the first, already solidified droplet, upon which it impinges. The solidification time depends, in addition to the thermal contact resistances at the interfaces, on the transport of heat through the solid structures above the flat wafer substrate. The total solidification time of the second droplet depends non-monotonically on the substrate temperature, initially increasing with decreasing substrate temperature. The impact velocities affect strongly the final shapes of the observed pile up structures. For decreasing Stefan number (i.e. higher substrate temperature) an increasing importance of wetting phenomena is observed.

Keywords: Droplet; Microscale; Solidification

1. Introduction

Droplets of various sizes and of a plethora of different fluids interacting with substrates of arbitrary shape appear in many areas of modern industrial applications. To exemplify, droplets of a molten material can be utilized as microscopic building blocks in the drop-wise manufacturing of structures such as in rapid prototyping or in microelectronics manufacturing [1–6]. Due to the very many naturally and industrially occurring droplet phenomena great scientific interest has been generated to improve understanding of droplet behavior, in particular in the engineering and physics communities. This interest has experienced a rapid growth recently due to the relevance of controlled microdroplet generation and deposition in a host of emerging technologies, such as microelectronics manufacturing and biotechnologies. Advancement and new implementations of such processes are only possible through a rigorous enhancement of the knowledge base associated to these processes. A multiplicity of physical phenomena has to be considered. The fluid mechanics involves a severely deforming free surface interacting with the substrate. The impact, recoiling and subsequent oscillations may also involve break up phenomena. It is also necessary to confront the very intricate field of wetting in the contact line region of the droplet. Thermodynamics poses several challenges

* Corresponding author. Tel.: +41-1-632-2738; fax: +41-1-632-1176.

E-mail address: dimos.poulikakos@ethz.ch (D. Poulikakos).

0017-9310/03/$ - see front matter
PII: S0017-9310(02)00289-2

Nomenclature

A	thermal contact area (m^2)
a_c	arc-length of contact line radius (m)
c_p	specific heat (J/kg K)
d	diameter (m)
E	thermal energy (J)
g	gravitational acceleration (m/s^2)
h	height (m)
k	thermal conductivity (W/m K)
L	latent heat of fusion (J/kg K)
$\dot{Q}$	heat transfer rate (W)
r	radius (m)
T	temperature (°C)
Δt	time period length (s)
t	time (s)
u	velocity component (m/s)
y	length/height (m)

Greek symbols

β	spread factor
γ	surface tension (N/m)
φ	angular deviation (°)
μ	dynamic viscosity (kg/ms)
ρ	density (kg/m^3)
ξ	viscous dissipation factor
ψ	contact angle (°)

Dimensionless numbers

Fr	Froude number ($u_0^2 d_0^{-1} g^{-1}$)
Ma	Marangoni number ($-\partial\gamma/\partial T(T_{1,0} - T_{2,0}) \times u_0^{-1}\ \mu^{-1}$)
Oh	Ohnesorge number ($We^{1/2} Re^{-1}$)
Pe	Peclet number ($RePr$)
Pr	Prandtl number ($\mu c_p k^{-1}$)
Re	Reynolds number ($\rho u_0 d_0 \mu^{-1}$)
Ste	Stefan number ($c_p(T_m - T_{2,0})L^{-1}$)
We	Weber number ($\rho u_0^2 d_0 \gamma^{-1}$)

Subscripts and superscripts

a	advancing
center	line of symmetry
eff	effective/lumped
m	melting
max	maximum
p	presolidified droplet
s	solid/solidification
0	initial condition
1	impinging droplet
2	presolidified droplet and wafer substrate
∞	final
β	spreading

when considering multiphase and multimode heat transfer. Chemistry can also come into play through various reactions from combustion to surface oxidation through adsorption.

Most works with focus on the deposition and the transient stages of the deformation and oscillation as well as the possible solidification process have been devoted to single droplets impinging on flat substrates [7,8]. As outlined above, there is also interest in structures built from individual droplets impacting on top of each other. Many times there exists the need to place more solder material in one position than that contained in a single droplet in chip packaging applications in microelectronics manufacturing. Since the reliable range of droplet sizes in solder jetting is rather limited, droplet pile up is a viable alternative. Unfortunately, there is very little information reported in the literature on droplet impact on non-flat substrates and pile-ups [1,4–6,9–11]. Che et al. [9] studied numerically the case of droplets impacting on top of each other. The solution method accounted for the conservation of mass, momentum, and energy both for the ambient, gaseous environment, the molten droplets, and the substrate. A fixed grid finite difference scheme was utilized in order to solve the equations numerically. A front-tracking method was employed in order to account for the free-surface and the solidification front. Issues like thermal contact resistance, the dynamic contact line, and the release of latent heat during solidification were neglected. No experimental results were reported to corroborate their numerical results. No surface structures like ripples were reported as has been shown and verified for single droplets impacting on flat substrates [12], exemplifying the limitations of this study. The work by Orme et al. [4–6,10] is focused on the employment of molten droplets in digital microfabrication. Thus, the work reports more on methods how to create objects by drop-wise build up and deposition strategies than on the prevailing physical phenomena. However, some analytical/numerical estimations on critical issues like splat cooling, remelting and thus adhesion between subsequent droplets are reported. Gao et al. [1] reported analytical estimates of cooldown and solidification time scales for columnar wax droplet deposition (i.e. pile up of many droplets). Liu et al. [11] reported numerical studies of droplets impacting on different non-flat substrates. The governing equations for transient, axisymmetric, viscous, incompressible flow, including surface tension effects were solved employing a modified version of RIPPLE [13]. The dynamic contact line, heat transfer and solidification were not considered. Free surfaces were modelled using the volume-of-fluid method. Sim-

ulations were performed using tungsten droplets with diameters in the range of 10–60 μm, at impact velocities of the order of O(100 m/s). The results show only fluid mechanical aspects of the impingement process including the splashing of the droplets. Regarding experiments on the pile up problem, transient visualizations/measurements are non-existent in the scientific literature.

An important subproblem in droplet deposition is that of surface wetting. The relevant issue is the dynamic contact line and the controversial determination of dynamic contact angles. Approaches to these problems span a wide area from continuum [14] down to molecular level [15–18] without conclusive results to date. Another related microscale problem is that of transient thermal contact resistance between an impacting microdroplet and a target object. Numerical simulations of droplet deposition processes require input parameters gained from comparing experimental visualizations with numerical simulations [7,8]. This pertains both to the issue of dynamic contact lines as well as thermal contact resistance between adjoining interfaces in the impact process.

The aim of this work is to shed more light on the complex interplay of the different phenomena occurring during the successive deposition (pile-up) of molten droplets. More specifically, the work is focused on the process in which a molten droplet impacts on a previously impacted and solidified droplet of the same material as shown schematically in Fig. 1. Only the axisymmetric case will be considered herein, which is of course in line with the actual printing approach in industrial applications where the printhead works on a "stop and drop" fashion. The work investigates eutectic melts since the majority of solder materials in electronics manufacturing are eutectic, exemplified by eutectic tin-lead solder (63% Sn–37% Pb). The focus will be on the fluid mechanics of the impact process, the heat transfer between the impinging and a predeposited already solidified droplet, the subsequent solidification of the molten material, and the related effect of substrate temperature on the process. The Reynolds and Weber numbers are O(100) and O(1) respectively. For molten eutectic solder droplets of picoliter size, this range corresponds to impact velocities and initial diameters of O(1 m/s) and O(100 μm). This is approximately the range covered by the industrial applications described above.

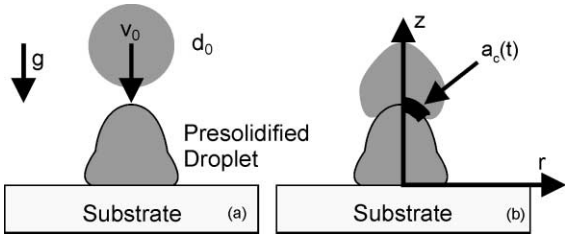

Fig. 1. Schematic of the pile up process studied in this investigation. (a) The impinging droplet is deposited ballistically on top of an already solidified droplet of the same material. (b) Spreading/recoiling of the impacted droplet on the presolidified droplet.

2. Experiments

2.1. Microdroplet generation

In order to investigate the transient pile up process, a series of droplet impact experiments with varying initial conditions were performed. The characteristic time-scale of the process can be estimated from experiments on flat substrates to be of the order of O(100 μs) [12,19–23]. The techniques employed to visualize the pile up process herein are an extension to those used by Attinger et al. [19] for single droplets impinging on a flat wafer substrate. Monodispersed picoliter-sized droplets on demand are generated utilizing a modified microdroplet jetting device manufactured by Microfab Inc., Dallas, TX. The main concept of the method stems from ink-jet technology. The droplet generation method can be briefly summarized as follows. By applying an electric pulse on a piezoelectric tube fitted concentrically around a glass capillary, picoliter size volumes of the corresponding fluid can be ejected from the glass tube on demand. The glass capillary is filled and in contact with a temperature controlled fluid reservoir. The latter is inertized and pressurized by nitrogen gas. Backpressure is needed to force the molten solder into the thin glass capillary since solder wets glass very poorly. The glass capillary features an orifice at the open end which focuses the pressure waves generated in the glass capillary by the piezoceramic tube and thereby enables the ejection of fluid ligaments [24]. The so created fluid volume initially oscillates upon ejection and assumes a spherical shape due to minimization of the interfacial energy. For a given fluid mostly the shape and time scales of the electric pulse applied to the piezoelectric tube, the inner diameter of the glass capillary, the diameter of the orifice, as well as the pressure level in the molten solder reservoir determine the size and the velocity of the so created droplets. The present investigation employs glass capillaries with an inner diameter of approximately 500 μm and an orifice diameter of approximately 58 μm, respectively. Thus, velocities and diameters can be changed by altering the driving electrical pulse and the backpressure. Respective ranges of approximately 50–100 μm for the droplet diameter and approximately 1–2.5 m/s for the impact velocity can be achieved in a repeatable manner. In order to minimize oxidation of the ejected solder droplets a covering co-flow of nitrogen is applied. The solder is melted and its temperature

controlled in the fluid reservoir by resistance heating. The temperature of the molten solder is kept at a constant temperature of 210 °C. The melting temperature of the latter is 183 °C.

2.2. Visualization method

The detailed and accurate visualization of a process taking place on a time scale on the order of O(100 μs) requires special attention. Conventional high-speed cameras are either limited to a certain frame acquisition frequency or the time window during which a very high acquisition frequency can be upheld. For example a very fast CCD camera as the KODAK EKTAPRO has a maximum acquisition rate of 40'500 frames per second at a very low resolution of 64×64 pixels. On the other hand, intensified CCD cameras can achieve time resolutions of up to 50 ns. However, only a limited amount of frames (8–30) can be recorded from a single event [25]. Other visualization methods such as strobe photography/videography rely on a different approach requiring a high repeatability of the investigated process [26–31]. The difference between high-speed camera and strobe techniques is that the former records the highest number of frames of a single event (i.e. the impact of a single droplet is recorded), whereas the latter reconstructs a single event from multiple, reproducible events by patching together several frames taken at subsequent times. Using this technique a time resolution on the order of O(1 μs) can be achieved. On this account, flash video microscopy was utilized in order to visualize the pile up process. To this end a triggered JAI M10 progressive scan CCD camera was employed for the digital imaging. Backlighting was provided by a triggered Xenon flash light unit (Hamamatsu L4634; Japan). An ICI-PCI framegrabber (Stemmer Imaging; Germany) was employed for the image recording. A microscope objective (Microtech Zoom 70, USA) was used to magnify the droplet images. An optical magnification of 29x on the CCD matrix plane was utilized giving a spatial resolution of 1.2 μm in the object plane.

2.3. Experimental setup and procedure

Based on the droplet generation and visualization methods described above, the experimental procedure consists in principle of electronically generating a sequence of pulse waveforms, which is then applied on the piezoceramic tube. Each individual pulse creates thereby a single droplet. Concurrently another sequence of pulses is generated to trigger the strobe flash/camera. In order to obtain a pile up structure, two droplets per acquired image are ejected subsequently. The first of these two droplets creates the presolidified solder droplet upon which the second droplet impacts. As substrate for the bottom droplet in the pile-up serves a gold coated

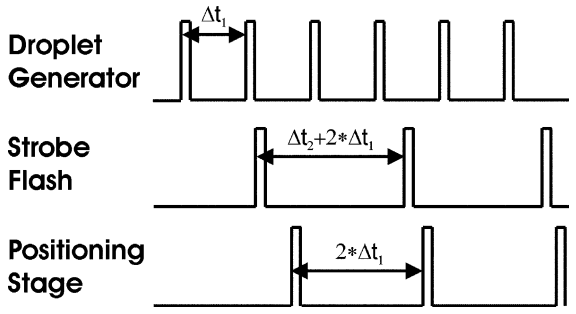

Fig. 2. Schematic of the trigger pulses deployed to drive and coordinate the droplet generator, the image acquisition, and the positioning stage.

silicon wafer situated underneath the droplet generator device. Images are only acquired upon impact of the second droplet. In order to provide a free wafer surface for each impacting droplet pair, a positioning stage is employed. The stage moves the wafer substrate in the focal plane of the camera a fixed distance after the creation of each pile up, halts, remains in position until the next pile up has been created and recorded, then moves on to the next position. This stage movement is controlled by a third, concurrent trigger pulse sequence. A schematic of these somewhat intricate trigger pulse sequences is shown in Fig. 2. Each experiment involves starting such a set of three trigger pulse sequences simultaneously. As shown in Fig. 2 different frequencies or period lengths are associated to the three pulse sequences. The droplets are created at a fixed frequency corresponding to a period length of Δt_1. The strobe flash and the camera are triggered at a lower frequency corresponding to a period length, which is twice the period length of the droplet generation, Δt_1, plus an adjustable time period Δt_2. The latter determines the time lag between the subsequent recorded frames of the second droplet motion in the pile up. This enables the piecing-together of a total event of the impact of the second droplet until its complete freezing, from a sequence of such frames each corresponding to a different but ideally identical pile up. Under the conditions of the above outlined experimental procedure it has to be emphasized, that this study focuses on the investigation of pile up structures built by two solder droplets having ideally exactly the same droplet diameter and impact velocity.

A schematic of the experimental setup is shown in Fig. 3. The x–y positioning is accomplished using an Aerotech MP100M (USA) and an Aerotech ALS130-150 (USA) fast precision stage. The travel distance from one pile up spot to the next is 200 μm. A LeCroy LW420 (USA) waveform generator is used to create the above described trigger sequences for the droplet generation and the image acquisition. Droplets are created at a

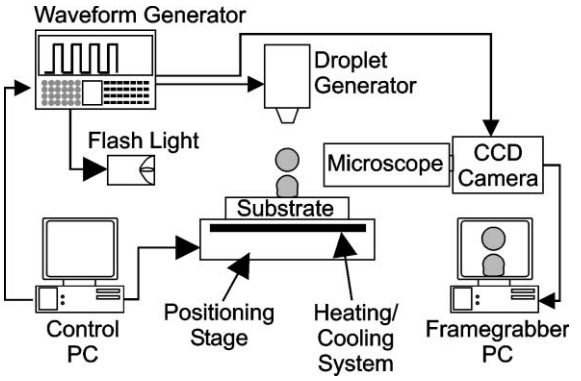

Fig. 3. Schematic of the experimental setup.

frequency of 8 Hz ($\Delta t_1 = 0.125$ s). The chosen time lag, Δt_2, between subsequent image acquisitions is 5 μs. The positioning stage is triggered at a frequency of 4 Hz.

The control of the substrate temperature involves a twofold system. The wafer substrate is heated by the droplet generator device by radiation and most of all by the hot nitrogen co-flow which flows at a rate of approximately 300 cm^3/min. In order to keep a constant and uniform wafer temperature below 70 °C the substrate has to be cooled. This is provided using a Lauda RCS (Instrumenten Gesellschaft AG, Germany) thermostat. Wafer temperatures above 70 °C are achieved using a resistive heater, temperature controlled by a Syrelec CTD 46 (Syrelec, France) controller device. To this end, the wafer substrate is fixed on a supporting copper plate mounted on the positioning stage. The copper plate carries a heater cartridge as well as channels for the cooling fluid from the thermostat. In order to improve thermal contact and to fix the wafer substrate on top of the supporting copper plate a thin layer of thermal paste (HTC Electrolube, England) is employed. The substrate is a semiconductor wafer (EM Marin; Switzerland) cut to rectangular sizes of approximately 10×100 mm. The wafer surface temperature is measured using a K-type thermocouple (Omega 304 SS9). The excess back pressure level in the molten solder reservoir is kept at a constant value of 6.9×10^3 Pa. The experimental setup is positioned in a dust free environment and on a vibration free table.

2.4. Experimental errors

A number of uncertainties and variations occur both in the postprocessing of the acquired impact sequences as well as in the experiments due to the visualization method and due to variations in the droplet generation. The experiment does not (ballistically) deliver perfect axisymmetric cases of the pile up. This is due to the fact that the trajectories of the ejected droplets have a slight, randomly distributed deviation from the ideal trajectory. There are a number of reasons responsible for this deviation. For situations where a thin liquid solder film or meniscus forms non-axisymmetrically around the orifice it has been observed that capillary forces deflect the ejected droplet prior to detachment from the orifice. Baggerman and Schwarzbach [32], using a similar droplet generator device as employed in this study, attributed this random horizontal component of the ejected droplet to system vibrations of the capillary/piezo ensemble. Nonetheless, this angular deviation was determined for different ejection velocities and droplet diameters by measuring the position of a large number of droplets at a distance of 1500 μm from the orifice. Independent of droplet velocity and diameter the angular deviation was determined to be $\varphi = 0.52° \pm 0.24°$. It has to be emphasized, that impacts randomly distributed and slightly off center have to be expected in the experiments. For presolidified droplet shapes not exhibiting very large radii of curvature in the area of impact this is acceptable. The reason for this is the fact that the Weber number of the droplets investigated in this study is on the order of O(1). This indicates that surface tension features a large restoring force to deformations in general and specifically to slight deformations due to three-dimensional effects. Clearly, for an increasing distance between the orifice and the substrate, an increasing departure from the ideal trajectory is obtained leading to unacceptable, strongly three-dimensional shapes. A means to minimize this problem is to decrease the distance between the substrate and the orifice. However, the molten solder, when ejected from the orifice features a tear-drop shape. Surface tension forces will drive an oscillatory fluid motion, damped by viscosity, to attain the energetically favorable shape of a sphere. The complexity of this effect is that droplets might impact in an ellipsoidal rather than a spherical shape. One may expect that this will lead to errors relative to the impact of an identical droplet of spherical shape since the field variables (i.e. pressure, velocities) differ from a droplet impacting in a non-oscillatory, spherical shape without gradients in the field variables [7,33,34]. The objective of this work is to investigate the axisymmetric pile up of a spherical droplet without important residual gradients in the field variables. Therefore, a trade-off situation is encountered between angular accuracy of the impinging droplets, and residual gradients in the field variables. After an iterative process, the chosen distance from the orifice to the substrate of 900 μm is a good compromise between positioning accuracy and damping of the oscillations induced by the droplet generation. Further problems of repeatability are encountered in the experimentally obtained velocities and diameters of the ejected droplets. Velocities were determined by measuring, for a fixed time delay, the

Table 1
Impact velocities and respective experimental errors

Velocity (m/s)	1.12	1.26	1.38	1.5	1.63	1.74
Error ± (m/s)	0.05	0.04	0.03	0.02	0.02	0.02
Error ± (%)	4.4	3.1	2.2	1.3	1.2	1.1

distance between two subsequent droplets shortly prior to impact. This was realized for a large number of droplets. Table 1, shows the errors for some velocities employed in the present study. The velocities are thereby averages of a large number of measurements. As can be seen in Table 1, the error increases with decreasing droplet velocity. This is in agreement with the observation that the stability of the entire jetting process deteriorates with decreasing jetting velocity or smaller electrical pulses on the piezoceramic actuator.

Simultaneously with the velocity measurements, variations in droplet diameter were monitored. It was found that independent of a specific velocity or particular average droplet diameter, a variation of approximately 2% of the initial droplet diameter occurred. This estimate includes the effect that the measurements are affected by further uncertainties. Measurement errors occur when evaluating distances on the acquired picture sequences. This pertains to values of the droplet diameter, pile up height, and the spreading distance of the impacting droplet. These uncertainties are largely due to operator errors in defining the edges of a droplet or specific points such as the contact line on the acquired image. It is very difficult to quantitatively determine this error. Therefore, an estimate for such errors of 1% of a measured distance is accepted based on repetitions of the same measurement.

An uncertainty connected with the error in the determination of the pile up height stems from the fact that the substrate level has to be determined form the recorded pictures. The cause for this is that the CCD camera, the light source and the substrate are not perfectly aligned leading to reflections of the pile up. This induces for certain pile up geometries errors when defining the locus of the substrate level. This error is estimated to be maximum 5% of the total pile up height including the error made when measuring distances as described above.

Additional uncertainties correspond to the thermal conditions for the experiments. First, the droplet temperature is assumed to be the one of the jetting device. An error estimate for the initial temperature of the droplet can be given based on the precision of the K-type thermocouple used to measure the device temperature, which is approximately 1 °C. However, the temperature is not measured exactly at the orifice due to implementation difficulties. On the other hand, the high thermal conductivity of the liquid metal (solder) assures the acceptability of the measurement. Second, the droplet is cooled convectively in-flight. However, based on work by Kang et al. [35] and Bennett and Poulikakos [36], who estimated this cooling with the Ranz–Marshal correlation [37], and the fact that the droplets travel for less than a millisecond in a covering nitrogen air-flow at a temperature close to the initial droplet temperature it is assumed that this convective cooling is negligible. Third, the actively cooled substrate is locally subjected to a stream of hot nitrogen from the inertizing co-flow. Measurements of the substrate surface temperature using a K-type thermocouple with a diameter of 0.25 mm showed a change in temperature in areas subjected to the hot nitrogen co-flow of approximately 2 °C, which is in the error range of the thermocouple. Changes of the thermal baseline conditions by the release of the thermal energy of the impinging droplets have found to be negligible [19].

Variations of impact velocity, initial diameter and also of thermal baseline conditions lead to a combined effect, which becomes, compared to single droplet impacts on flat substrates, sometimes observable in visualizations of the pile up process.

3. Results

3.1. Experimental conditions

In terms of dimensional values, sequences at different impact velocities and substrate temperatures were recorded using flash video microscopy. In addition, end shapes of pile-ups were imaged by scanning electron microscopy (Hitachi, S-900) in order to obtain fine surface structures. Two series of experiments were performed covering the influence of the impact velocity and, for constant impact velocity, the influence of the substrate temperature on the pile up process.

For all experiments the droplet diameter was kept at approximately 80 μm. This is due to the fact that at this diameter the most stable droplet generation was achieved. The visualized experimental cases are given in Table 2.

3.2. The spreading process

Upon formation of contact between the impinging droplet and the presolidified droplet on the substrate the liquid starts to spread outward. As mentioned by Rein [33], different scenarios depending on the kinetic energy of the droplet are possible. In the present study with $We > 1$, spreading is greatly influenced by the kinetic energy. Concurrently, surface tension forces resist and viscous forces damp the spreading process. Furthermore, solidification influences the spreading process as

Table 2
Initial conditions of the experimental cases investigated[a]

Case	Impact velocity, u_0 (m/s)	Droplet diameter, d_0 (μm)	Substrate temperature, $T_{2,0}$ (°C)	Reynolds number, *Re*	Weber number, *We*	Stefan number, *Ste*	Ohnesorge number, *Oh*	Prandtl number, *Pr*
1	1.51 ± 0.02	76.83 ± 1.5	25 ± 2	363.89	4.17	0.895	0.0056	0.025
2	1.50 ± 0.02	77.22 ± 1.4	50 ± 2	363.31	4.14	0.754	0.0056	0.025
3	1.50 ± 0.02	77.03 ± 1.5	75 ± 2	362.42	4.13	0.612	0.0056	0.025
4	1.51 ± 0.02	76.17 ± 1.5	100 ± 2	360.77	4.14	0.470	0.0056	0.025
5	1.52 ± 0.02	75.02 ± 1.5	125 ± 2	357.67	4.13	0.329	0.0056	0.025
6	1.49 ± 0.02	76.83 ± 1.5	150 ± 2	359.07	4.06	0.187	0.0056	0.025
7	1.12 ± 0.05	80.10 ± 1.6	25 ± 2	281.39	2.39	0.895	0.0054	0.025
8	1.26 ± 0.04	76.83 ± 1.5	25 ± 2	303.65	2.91	0.895	0.0056	0.025
9	1.38 ± 0.03	79.59 ± 1.5	25 ± 2	344.51	3.61	0.895	0.0055	0.025
10	1.51 ± 0.02	76.83 ± 1.5	25 ± 2	363.89	4.17	0.895	0.0056	0.025
11	1.63 ± 0.02	77.51 ± 1.5	25 ± 2	396.29	4.91	0.895	0.0056	0.025
12	1.74 ± 0.02	83.03 ± 1.6	25 ± 2	453.16	5.99	0.895	0.0054	0.025

Cases 1–6 represent the thermal regime with changing initial substrate temperatures and cases 7–12 represent the impact regime with changing impact velocities.

[a] Values of the Reynolds, Weber, Stefan, and Ohnesorge number correspond to averaged values of the impact velocity, the initial diameter and the temperature.

well. This can take place by solidification at the wetting line [38,39] or by annihilation of kinetic energy by solidification [40]. Based on droplet impact studies on flat substrates Bennett and Poulikakos [41] proposed that surface tension effects dominate the termination of the droplet spreading over viscous effects when:

$$We \ll 2.8Re^{0.457} \tag{1}$$

In their scaling arguments the effect of solidification in the droplet spreading was neglected. Based on the values of the characteristic dimensionless numbers of the pile up cases in this study, Table 2, the right-hand side of Eq. (1) is about an order of magnitude larger than the Weber number. This points at a dominance of the surface tension forces in the termination of the spreading process. On the other hand, neglecting the presence of thermal contact resistance, Schiaffino and Sonin [42] derived upon scaling analysis an estimate of the ratio of the spreading time, t_β, and the solidification time, t_s:

$$\frac{t_\beta}{t_s} = \frac{OhSte}{Pr} \tag{2}$$

Based on the values of the characteristic dimensionless numbers in Table 2, the ratio given by Eq. (2) is in the range of 0.04–0.2. Accounting for thermal contact resistance it is expected that this ratio would be further decreased. This means that spreading is a process featuring a markedly shorter time scale than the solidification process. However, local freezing at the wetting line is expected to occur markedly earlier than bulk freezing. Based on the above scaling, spreading arrest should be controlled by surface tension forces unless solidification at the wetting line occurs and terminates the spreading. Representative examples of reconstructed pile up sequences are shown in Figs. 4 and 5, containing cases 1 and 5. As visible in those figures viscosity has a low influence on the transient motion of the impacting droplet, i.e. the motion is only weakly damped. Furthermore, solidification effects become only visible after the first oscillation cycle. The difference in the final shapes of the pile ups in Figs. 4 and 5 caused solely by the effect of the substrate temperature is indeed remarkable and will be addressed in detail later in this paper.

A quantitative measure of the temporal evolution of the spreading process is the spread factor β, which can be expressed as follows:

$$\beta(t) = \frac{a_c(t)}{r_0} \tag{3}$$

where a_c is the instantaneous travel distance of the contact line and r_0 is the initial droplet radius as shown in Fig. 1(b). The instantaneous travel distance of the contact line, a_c, is measured in terms of the arc-length from the center of impact along the free-surface of the presolidified droplet to the contact line. Defining the instantaneous travel distance of the contact line in this manner, takes the curvature of the presolidified droplet into account. Thus, it renders results comparable to already existing results for droplets impacting on flat substrates. To this end, the surfaces of the presolidified droplets for all cases given in Table 2 were digitized in order to derive an expression for the arc-length. It has to be emphasized, that this approach is somewhat critical following the arguments on accuracy and repeatability

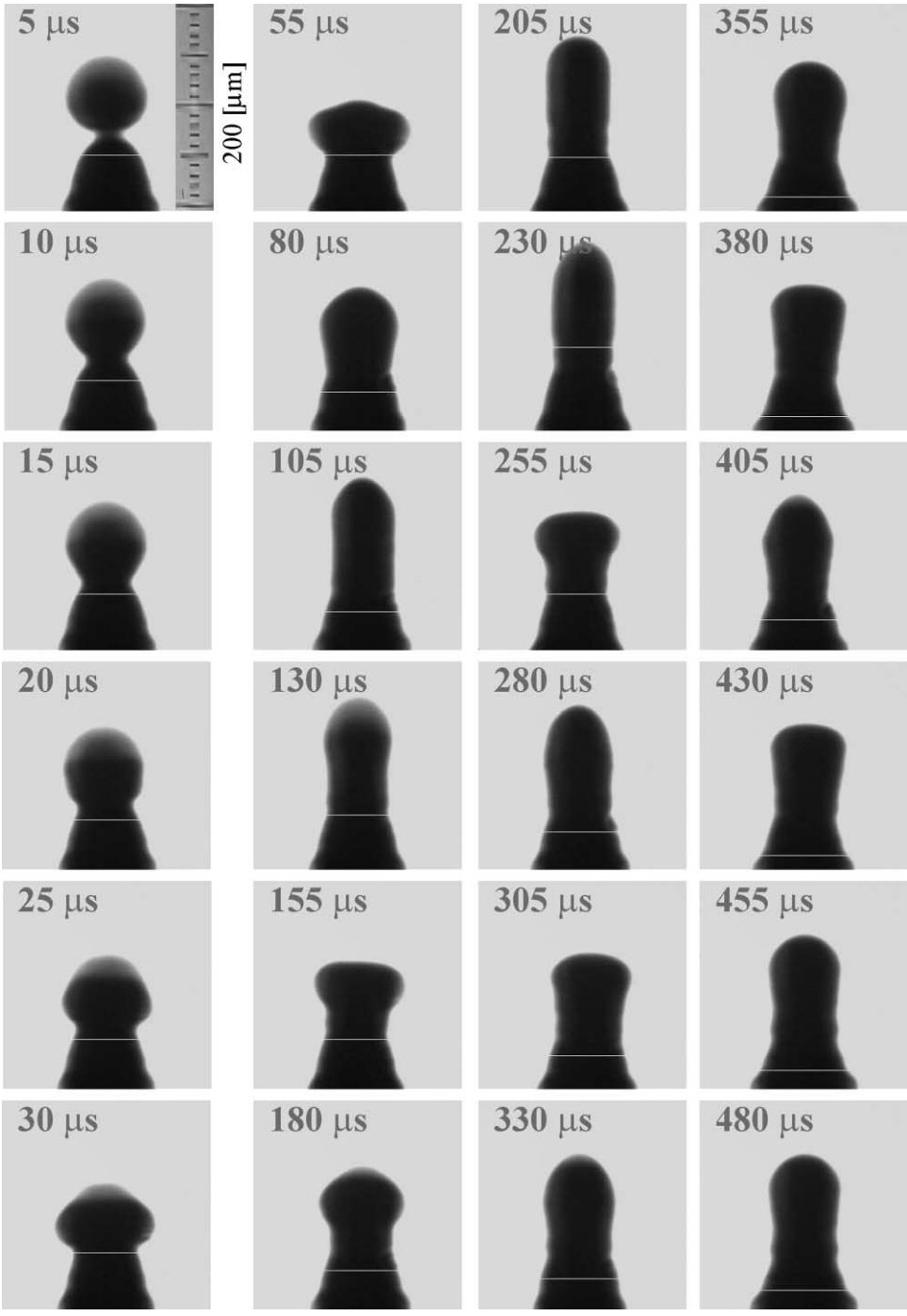

Fig. 4. Case 1, spreading, oscillation, and solidification during a pile up. Initial conditions: $u_{z0} = 1.51 \pm 0.02$ m/s, $d_0 = 76.83 \pm 1.54$ μm, $T_{1,0} = 210$ °C, $T_{2,0} = 25$ °C.

in Section 2.4. As follows upon inspection of Table 3, the parameter changed for the thermal series (cases 1–6) is the substrate temperature (affecting the Stefan number,) whereas for the impact series (cases 7–12) the impact velocity (affecting the Reynolds and Weber numbers) is varied.

Fig. 6 shows the temporal evolution of the spread factor as a function of the initial substrate temperature,

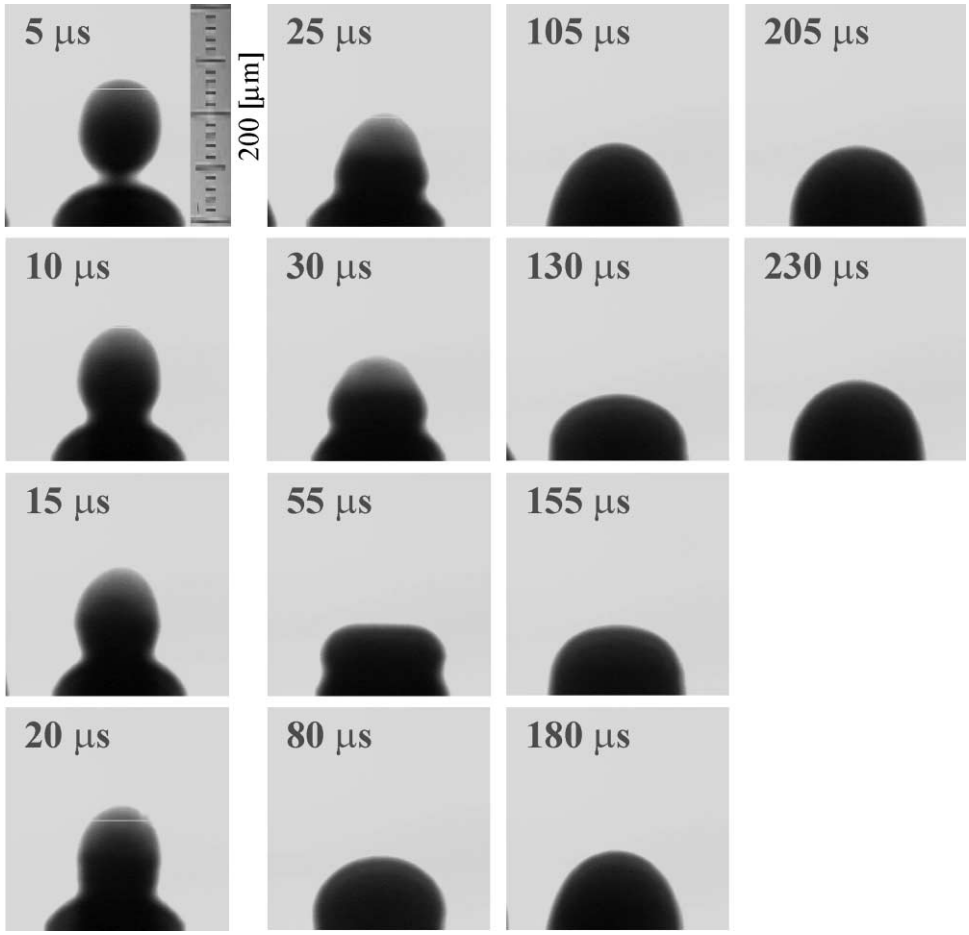

Fig. 5. Case 5, spreading, oscillation, and solidification during a pile up. Initial conditions: $u_{z0} = 1.52 \pm 0.02$ m/s, $d_0 = 75.02 \pm 1.5$ μm, $T_{1,0} = 210$ °C, $T_{2,0} = 125$ °C.

Table 3
Spread factors β_{max} and β_∞ as well as the spread factors ratio β_∞/β_{max} for all experimental cases investigated

Case	Impact velocity, u_0 (m/s)	Droplet diameter, d_0 (μm)	Substrate temperature, $T_{2,0}$ (°C)	Spread factor, β_{max}	Spread factor, β_∞	Spread factor ratio, β_∞/β_{max}
1	1.51 ± 0.02	76.83 ± 1.54	25	1.0370	1.0203	0.9839
2	1.50 ± 0.02	77.22 ± 1.54	50	1.2329	1.0897	0.8839
3	1.50 ± 0.02	77.03 ± 1.54	75	1.1998	1.0829	0.9026
4	1.51 ± 0.02	76.17 ± 1.52	100	1.4641	1.4269	0.9746
5	1.52 ± 0.02	75.02 ± 1.50	125	1.8426	1.8305	0.9934
6	1.49 ± 0.02	76.83 ± 1.54	150	1.8374	1.8212	0.9912
7	1.12 ± 0.05	80.10 ± 1.60	25	1.0690	1.002	0.9373
8	1.26 ± 0.04	76.83 ± 1.54	25	1.0306	0.9413	0.9134
9	1.38 ± 0.03	79.59 ± 1.59	25	1.0916	0.9807	0.8984
10	1.51 ± 0.02	76.83 ± 1.54	25	1.0370	1.0203	0.9832
11	1.63 ± 0.02	77.51 ± 1.55	25	1.2403	1.1327	0.9132
12	1.74 ± 0.02	83.03 ± 1.66	25	1.8611	1.8072	0.9710

cases 1–6. The maximum spread factor β_{max} and the final spread factor β_∞ pertaining to the solidified contact line are given in Table 3.

Due to the different initial substrate temperatures in cases 1–6, the presolidified droplets, upon which the second droplets in the pile up impact, feature different

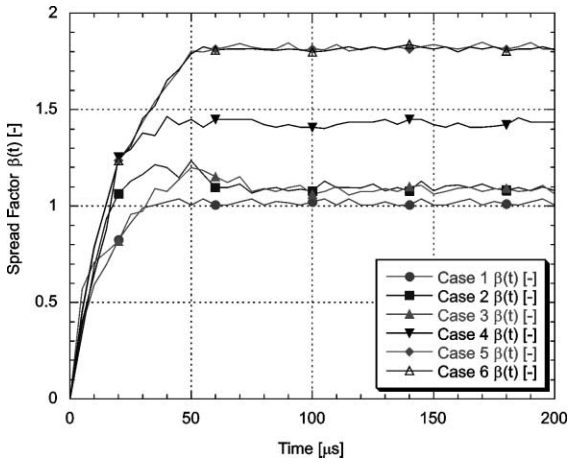

Fig. 6. Spread factor $\beta(t)$ for the cases pertaining to the thermal regime.

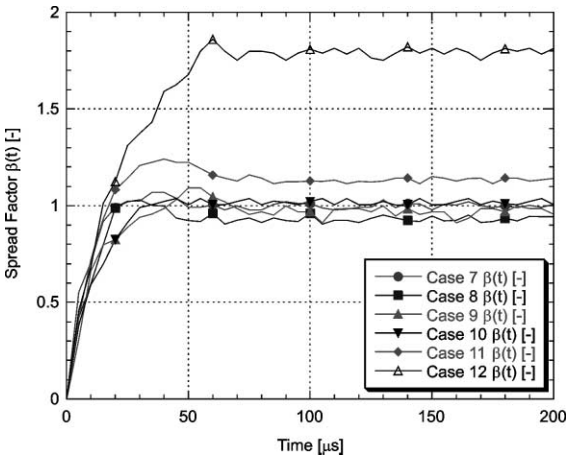

Fig. 7. Spread factor $\beta(t)$ for the cases pertaining to the impact regime.

shapes. As can be seen in Fig. 6 the initial stage of the spreading process is already different for all cases. After less than 10 μs the temporal evolution of the spread factor β diverges. This differs markedly from findings by Attinger et al. [19] on approximately identical droplets impinging on a flat, wafer substrate (the same as deployed in this study) at different initial temperatures. The difference in spreading behavior is due to the fact that the specific shapes of the presolidified droplets (determined by the different substrate temperatures) have a noticeable influence on the spreading of an impinging droplet. In other words, the substrate temperature effect on the spreading of the second droplet manifests itself in an implicit manner, through the surface curvature of the presolidified first droplet.

In the thermal regime (cases 1–6), the cases 4, 5, and 6 adopt a special character. As their initial substrate temperatures lie in the range of 100–150 °C the presolidified droplets feature very similar lens shapes with small curvature effects as shown in Fig. 5 for case 5. The spreading behavior for these cases is comparable and not strongly dependent on the specific substrate shape, as can be seen by the less diverging evolution of the spread factor β in Fig. 6. Attinger et al. [19] reported similar results for solder droplets impacting on flat substrates. They showed that the spread factor β is independent of the Stefan number for $Ste < 0.48$, corresponding to an initial substrate temperature of 98 °C. Similar independence is observed in this study for cases 5 and 6, however, for Stefan numbers $Ste < 0.33$. Another finding of Attinger et al. [19] was that both β_{max} and β_{∞} increase with decreasing Stefan number (increasing initial substrate temperature) until $Ste \approx 0.48$. This is also true for the cases 5 and 6 in this study the characteristic Stefan number having a smaller value, $Ste \approx 0.33$.

Fig. 7 shows the temporal evolution of the spread factor as a function of the impact conditions (i.e. *Re* and *We* number), cases 7–12. The maximum spread factor β_{max} and the final spread factor β_{∞} are also given in Table 3. As follows from inspection of Tables 2 and 3 the droplets feature impact velocities in the range of 1.12–1.74 m/s with approximately the same diameter of 80 μm. Similarly to the thermal regime, the evolution of the spread factor between the different cases diverges shortly upon formation of contact between the impinging and the presolidified droplet. Due to the different impact velocities (impact kinetic energy) this has to be expected. Increasing the impact velocity, respectively Reynolds and Weber number, should also lead to larger values of the maximum spread factor β_{max} and the final spread factor β_{∞} as in the impact of droplets on flat substrates [21,43,44]. When comparing the values of the maximum spread factor β_{max} and the final spread factor β_{∞} for the present pile up cases of the impact regime, Fig. 7 and Table 2, it is apparent, that this is not unequivocal. Whereas for higher impact velocities this argument holds, cases 11 and 12, at lower impact velocities, cases 7–10, the dependence of β_{max} on the impact velocity is not monotonic. The maximum spread factor β_{max} and the final spread factor β_{∞} thus show a dependence on the substrate shape.

Another avenue to investigate the importance of the substrate shape on the spreading is to compare the experimentally obtained maximum spread factors β_{max} with analytical models, which neglect effects of substrate curvature among other things. A large number of such approximate analytical and experimentally matched models, relating the maximum spread factor β_{max} to the predominant dimensionless numbers, exist in the literature [7,40,41,43,45]. These analytical models are derived by order of magnitude arguments scaling the effect of

surface tension, viscous forces/dissipation, inertial forces, gravity forces and some also account for solidification effects as well as the Marangoni effect on the spreading extent. The most versatile model accounting for solidification but not the Marangoni effect is due to Pasandideh-Fard et al. [40]:

$$\beta_{\max} = \sqrt{\frac{We + 12}{3(1 - \cos\psi_a) + 4We/\sqrt{Re} + We\sqrt{(3Ste)/(4Pe)}}} \tag{4}$$

where ψ_a is the advancing dynamic contact angle. Another versatile model for the maximum spread factor not accounting for solidification but taking the Marangoni and gravitational effects into account is due to Attinger et al. [46]:

$$\frac{1}{12}\left(1 + \frac{1}{Fr}\right) + \frac{1}{We} = \frac{1}{\beta_{\max}^2}\left(\frac{1}{18Fr}\right) + \beta_{\max}^2(1 - \cos\psi_a)\left(\frac{1}{4We} + \frac{Ma}{6Re}\right) + \beta_{\max}^2\frac{\xi}{\sqrt{Re}} \tag{5}$$

where ξ is the viscous dissipation factor. Based on the experimental baseline conditions given in Table 2, these models predict the maximum spread factor $\beta_{\max}$ as presented in Fig. 8(a) and (b). The analytical models predict maximum spread factors $\beta_{\max}$ monotonically and weakly increasing with the Reynolds numbers. Comparing the experimentally obtained values in the impact regime with the analytical scaling laws, Fig. 8(a), shows first that the analytical models for a flat substrate tend to overpredict the maximum spread factor $\beta_{\max}$. The experimental values of $\beta_{\max}$ show a much stronger dependence on the Reynolds number than the approximate analytical predictions for flat substrates. In the thermal regime, Fig. 8(b), the experimental values of $\beta_{\max}$ also show a much stronger dependence on the Stefan number than the approximate analytical predictions for flat substrates. This further underlines the importance of the substrate shape or curvature on the spreading behavior of an impinging droplet. The average advancing contact angle in Eqs. (4) and (5) was estimated to be $\psi_a = 135°$ following the experimental results by Attinger et al. [19]. For simplicity and since the models are only of approximate nature, this value was used for all cases of the impact regime. Other estimates for the averaged advancing contact angle led to slightly different values of the maximum spread factor but not to different trends concerning the dependence on both the Reynolds and the Stefan number. The dissipation factor ξ in Eq. (5) depends on the assumed value of the boundary thickness and was estimated to be $\xi = 0.547$ [19]. Furthermore, the Marangoni number in Eq. (5) was calculated employing a constant temperature coefficient of the surface tension of -0.1833 mN/m K, according to the experimental results by Carroll and Warwick [47].

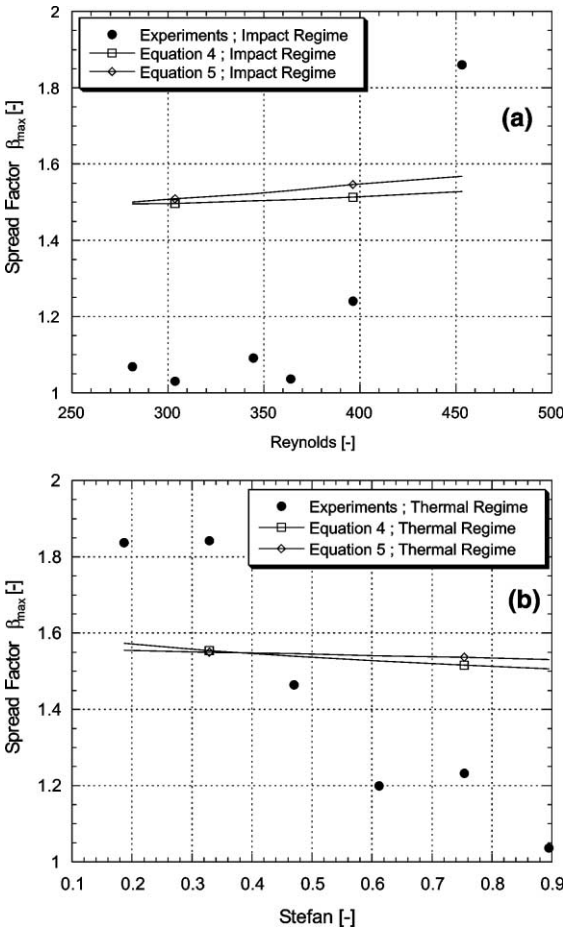

Fig. 8. Comparison of the experimentally determined maximum spread factor $\beta_{\max}$ with the analytical models, Eqs. (4) and (5), in function of: (a) the Reynolds number and (b) the Stefan number.

3.3. The solidification process

The solidification times are determined experimentally, based on visual observation. The motion of the impinging droplet is halted by solidification and not by viscous dissipation. The end of the droplet oscillations, as observed for instance in the pile up sequences in Figs. 4 and 5, indicates the termination of the solidification process. Quantitative information on the solidification can thus be extracted from the motion of the droplet top $y_{\text{center}}(t)$. Fig. 9 shows the motion of the latter for cases 3, 6, and 9. The solidification time t_s is defined as the instance where the height $y_{\text{center}}(t)$ of the pile up structure remains constant (within $\pm 2\%$ of the initial droplet

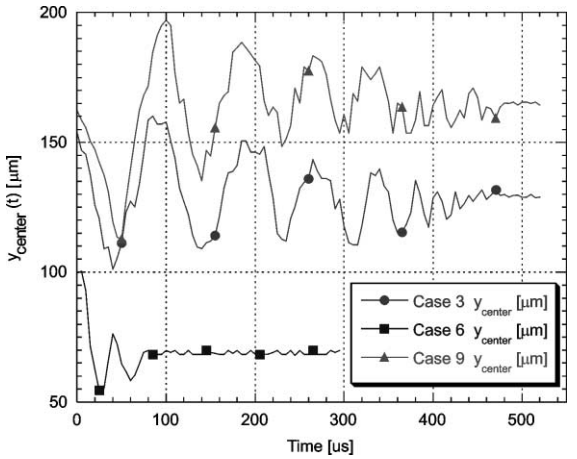

Fig. 9. Damped oscillatory motion of the droplet top $y_{\text{center}}(t)$ for the cases 3, 6, and 9.

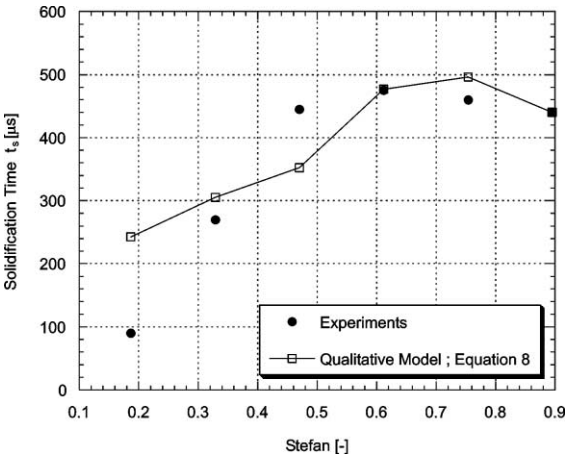

Fig. 10. Experimentally determined solidification times for the thermal regime (cases 1–6) compared to the analytical model, Eq. (6), and the qualitative solidification model, Eq. (8), in function of the Stefan number.

diameter) for a time length more than half a period of its oscillations [19]. Table 4 shows a compilation of the experimentally determined solidification times t_s for all cases.

The error in determining the above solidification times is estimated to be $-10/+30$ μs. This estimate is based upon the following reasoning and with an experimental time resolution of 5 μs in the visualization procedure. The apparent termination of the oscillation motion can be located with an accuracy of approximately ± 2 frames of the visualized pile up sequence, thus ± 10 μs. Due to the difficulty to distinguish small amplitudes of the oscillations just prior to complete solidification, there is a bias to assume that solidification occurs earlier than in reality. Therefore, the upper limit is extended to 6 frames, thus $+30$ μs.

Comparing with the solidification times measured by Attinger et al. [19] on practically identical droplets impacting on flat substrates at approximately the same temperatures, it is apparent that solidification times of the second droplet of a pile up are about 30% larger. Furthermore, it was reported in [19] that the solidification time featured a non-monotonic dependence on the Stefan number showing a single minimum at about 90 °C in a thermal regime ranging from 48 to 135 °C. Fig. 10 shows the dependence of the solidification time on the Stefan number (cases 1–6). The experimental finding that droplets impacting with practically the same initial velocity and diameter solidify slower with increasing Stefan numbers (increasing the temperature difference between the warm droplet and the colder substrate by decreasing the substrate temperature) is initially surprising. The solidification time features a maximum over the range of Stefan number investigated. This behavior was elucidated qualitatively using a simple analytical model accounting for the physics involved. Assuming that heat is transferred from the top droplet to the substrate via conduction through the bottom droplet the following approximate model is postulated:

$$\dot{Q} = k_{\text{eff}} A \frac{T_{1,0} - T_{2,0}}{h_{\text{p}}} \tag{6}$$

where k_{eff} is an effective thermal conductivity of the presolidified droplet, A is the area of the interface between the presolidified droplet and the wafer substrate, and h_{p} is the height of the presolidified droplet. The initial thermal energy of the impinging droplet can be expressed as follows:

$$E = \frac{\rho \pi d_0^3}{6} [c_{\text{p},1}(T_{1,0} - T_{\text{m}}) + L] \tag{7}$$

The solidification time can then be expressed as follows:

$$t_{\text{s}} = \frac{E}{\dot{Q}} = \frac{\rho \pi d_0^3 [c_{\text{p},1}(T_{1,0} - T_{\text{m}}) + L] h_{\text{p}}}{6 k_{\text{eff}} A (T_{1,0} - T_{2,0})} \tag{8}$$

Table 4
Experimentally determined solidification times t_s

Case	1	2	3	4	5	6	7	8	9	10	11	12
t_s (μs)	440	460	475	445	270	90	450	425	480	440	500	435

Inspection of Eq. (8) clearly shows that while decreasing the substrate temperature would decrease the solidification time, there is the effect of other parameters, which simultaneously vary because they depend on the substrate temperature, that needs to be accounted for. A decrease in the substrate temperature increases h_p and decreases A. Both these variations would tend to increase the solidification time. Hence, a non-monotonic behavior of the solidification time on the substrate temperature is to be expected.

Based on the values for the thermal regime (cases 1–6), the dependence of the solidification time on the Stefan number, from Eq. (8), is shown as a solid line in Fig. 10. This result is only meant to illustrate the non-monotonic trend featuring a local maximum as explained earlier. The effective thermal conductivity in Eq. (8) was selected arbitrarily so that the analytical result for $Ste = 0.9$ matched the experimental result. The so determined value of the effective thermal conductivity is $k_{eff} = 20.5$ W/m K. Accounting for thermal contact resistance between the presolidified droplet and the wafer substrate this value seems however reasonable compared to the thermal conductivity of solid solder ($k = 48$ W/m K).

The overall effect of the substrate temperature (thermal regime) as well as of the impact velocity (impact regime) on the attained pile up endshapes is shown in Fig. 11(a) and (b). Clearly, in the thermal regime, an increase of the solidified contact area (see also Fig. 6) as well as a decrease of the final height with increasing substrate temperature is visible. This increase in the contact area is associated to retardation effects in the solidification as well as changes of the substrate wettability due to the increasing substrate temperature. This means that the importance of capillary effects become, even in a typically impact-inertia dominated regime as in this study, increasingly important with increasing substrate temperatures. Wetting experiments using metal droplets on metal surfaces (not of the same material) have shown that an increase of the substrate temperature

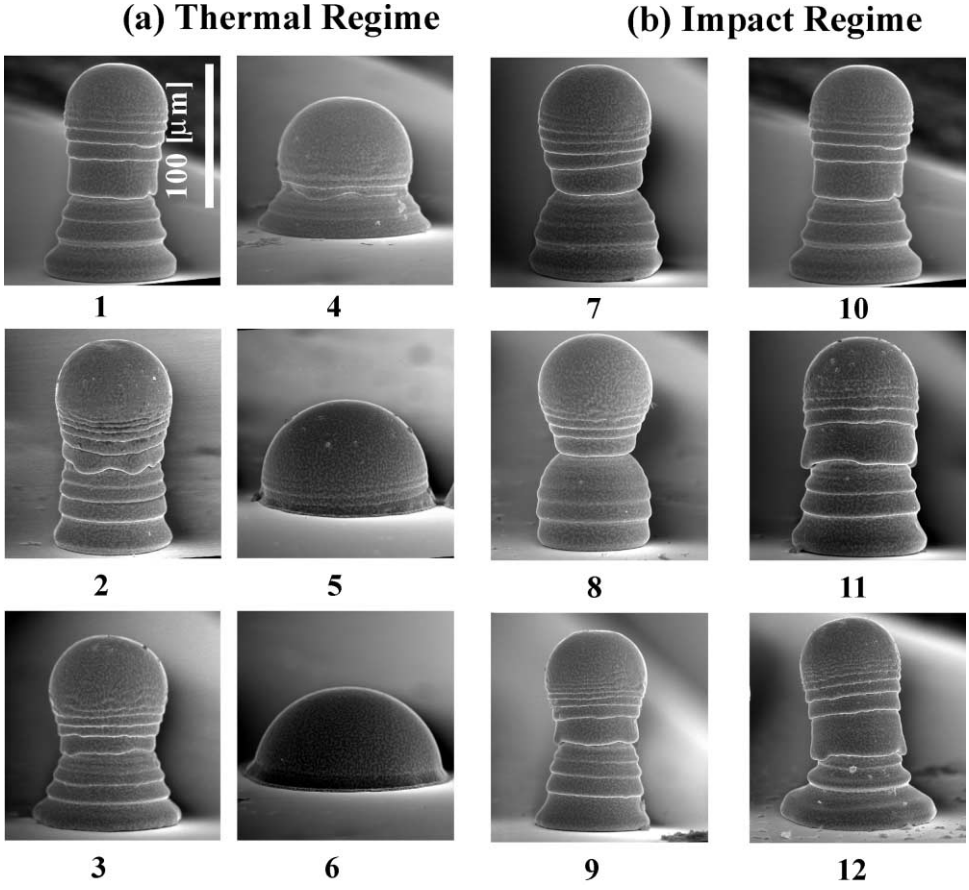

Fig. 11. Compilation of the attained pile up endshapes for the thermal and the impact regime. The numbers in the lower, right corner correspond to the case numbering given in Table 2.

usually leads to an increased wettability [48]. Furthermore, it has been observed that the spreading time of a droplet depends logarithmically on temperature and that the time decreases with increasing temperature [48]. Similar results were obtained for 60Sn40Pb solder droplets on gold–platinum metal films [49]. The above referenced experiments relied basically on gently placing macroscopic metal droplets on respective metal substrates. Thus, spreading of the droplets was controlled by capillarity. No experiments covering the material system of the present study could be found in the scientific literature. Nonetheless, the above referenced experimental observations point to a possible explanation for the increasing final spread factors with decreasing Stefan numbers.

The set of pile up cases of the impact regime, cases 7–12 in Fig. 11(b), shows endshapes of pile up structures created at identical thermal baseline conditions with only the impact velocity varying. As can be clearly seen, the shapes depend in a complex manner on the initial impact velocity. Variations in the impact velocity lead to different deformations and spreading rates as well as final spread factors. The temporal evolution of the contact area leads concurrently to different cooling rates of the impinging droplet. The simultaneously occurring solidification process captures different shapes during the transient motion of the impacting droplet.

4. Summary

To the best of our knowledge, this work presents the first experimental results on the transient fluid dynamics, wetting and solidification of molten microdroplets impinging on presolidified droplets or in more general terms on non-flat substrates of the same material. The experimental results point to a noticeable influence of the substrate (presolidified droplet) shape on both the spreading and the solidification process occurring during a microdroplet pile up. The spreading behavior seems to be influenced by the specific surface curvature of the presolidified droplet compared to the spreading behavior of droplets impinging on flat substrates. The effect of substrate temperature and the related capillary phenomena on the final pile up shape is proven to be significant. Accounting for conduction through the presolidified droplet aids the understanding of the non-monotonic dependence of the solidification time on the Stefan number.

Acknowledgements

This work has been partially supported by the Swiss National Science Foundation, grant no. 21-49183.96.

Appendix A. Relevant thermophysical properties

	Material	
	Solder (liquid)	Solder (solid)
K (W/m K)	25	48
μ (Pa s)	0.00262	–
ρc_p (kJ/m^3 K)	1750	1450.2
ρ (kg/m^3)	8218	8240
γ (N/m)	0.345	–
T_m (°C)	183	183
L (J/kg)	42,000	42,000
c_p (J/kg K)	238	176

Properties can be found in CRC Handbook of Chemistry and Physics [50].

References

[1] F. Gao, A. Sonin, Precise deposition of molten microdrops: the physics of digital microfabrication, Proc. R. Soc. Lond. A 444 (1994) 533–554.
[2] L.J. Zarzalejo, K.S. Schmaltz, C.H. Amon, Molten droplet solidification and substrate remelting in microcasting Part I: Numerical modeling and experimental verification, Heat Mass Transfer 34 (1999) 477–485.
[3] J.P. Kruth, Material incress manufacturing by rapid prototyping techniques, Ann. CIRP 40 (2) (1991) 603–614.
[4] M. Orme, A novel technique of rapid solidification net-form materials synthesis, J. Mater. Eng. Perform. 2 (3) (1993) 399–405.
[5] M. Orme, C. Huang, J. Courte, Deposition strategies for control of microstructures microporosity and surface roughness in droplet-based solid freeform fabrication of structural materials, in: E.F. Matthys, W.G. Truckner (Eds.), Melt Spinning, Strip Casting and Slab Casting, The Minerals, Metals and Materials Society, Warrendale, PA, 1996, pp. 125–143.
[6] M.E. Orme, C. Huang, J. Courter, Precision droplet-based manufacturing and material synthesis, Atomization Sprays 6 (1996) 305–329.
[7] S. Haferl, Z. Zhao, J. Giannakouros, D. Attinger, D. Poulikakos, Transport phenomena in the impact of a molten droplet on a surface: macroscopic phenomenology and microscopic considerations Part I: Fluid dynamics, in: C.-L. Tien (Ed.), Annual Reviews in Heat Transfer, Begell House, New York, 2000, pp. 65–143.
[8] D. Attinger, S. Haferl, Z. Zhao, D. Poulikakos, Transport phenomena in the impact of a molten droplet on a surface: macroscopic phenomenology and microscopic considerations Part II: Heat transfer and solidification, in: C.-L. Tien (Ed.), Annual Reviews in Heat Transfer, Begell House, New York, 2000, pp. 145–205.
[9] J. Che, S. Ceccio, G. Tryggvason. Computations of structures formed by the solidification of impinging molten metal drops, in: 1999 TMS Annual Meeting, San Diego, CA, February 1999.

[10] M. Orme, R. Smith, Enhanced aluminum properties with precise droplet deposition, ASME J. Manufact. Sci. Eng. 122 (2000) 484–493.
[11] H. Liu, E.J. Lavernia, R.H. Rangel, Modeling of molten droplet impingement on a non-flat surface, in: 1994 International Mechanical Engineering Congress and Exposition, Chicago, IL, 1994.
[12] J.M. Waldvogel, D. Poulikakos, Solidification phenomena in picoliter size droplet deposition on a composite substrate, Int. J. Heat Mass Transfer 40 (1997) 295–309.
[13] D.B. Kothe, R.C. Mjolsness, M.D. Torrey, RIPPLE: A computer program for incompressible flows with free surfaces, LA-12007-MS, UC-000 Los Alamos National Laboratory, New Mexico, 1991.
[14] S.F. Kistler, Hydrodynamics of wetting, in: J.C. Berg (Ed.), Wettability, Dekker, New York, 1993.
[15] J. Koplik, J.R. Banavar, J.F. Willemsen, Molecular dynamics of poiseuille flow and moving contact lines, Phys. Rev. Lett. 60 (1988) 1282–1285.
[16] J. Koplik, J.R. Banavar, J.F. Willemsen, Molecular dynamics of fluid flow at solid surfaces, Phys. Fluids A 1 (1989) 781–794.
[17] P.A. Thompson, M.O. Robbins, Simulations of contact-line motion: slip and the dynamic contact angle, Phys. Rev. lett. 63 (1989) 766–769.
[18] P.A. Thompson, S.M. Troian, A General boundary condition for liquid flow at solid surfaces, Nature 389 (1997) 360–362.
[19] D. Attinger, Z. Zhao, D. Poulikakos, An experimental study of molten microdroplet surface deposition and solidification: transient behavior and wetting angle dynamics, ASME J. Heat Transfer 122 (2000) 544–556.
[20] Z. Zhao, D. Poulikakos, J. Fukai, Heat transfer and fluid dynamics during the collision of a liquid droplet on a substrate: I-modeling, Int. J. Heat Mass Transfer 39 (1996) 2771–2789.
[21] Z. Zhao, D. Poulikakos, J. Fukai, Heat transfer and fluid dynamics during the collision of a liquid droplet on a substrate I. Experiments, Int. J. Heat Mass Transfer 39 (1996) 2791–2802.
[22] J.M. Waldvogel, D. Poulikakos, Solidification phenomena in picoliter size solder droplet deposition on a composite substrate, Int. J. Heat Mass Transfer 40 (2) (1997) 295–309.
[23] J.M. Waldvogel, D. Poulikakos, D.B. Wallace, R. Marusak, Transport phenomena in picoliter size solder droplet dispension on composite substrate, J. Heat Transfer 118 (1996) 148–156.
[24] J.F. Dijksman, Hydrodynamics of small tubular pumps, J. Fluid Mech. 139 (1984) 173–191.
[25] C.D. Ohl, A. Philipp, W. Lauterborn, Cavitation bubble collapse studied at 20 million frames per second, Annalen der Physik 4 (1) (1995) 26–34.
[26] S. Chandra, C.T. Avedisian, On the collision of a droplet with a solid surface, Proc. R. Soc. Lond. A 432 (1991) 13–41.
[27] C.D. Stow, M.G. Hadfield, An experimental investigation of fluid flow resulting from the impact of a water drop with an unyielding dry surface, Proc. R. Soc. Lond. A 373 (1981) 419–441.
[28] L.H. Wachters, N.A.J. Westerling, The heat transfer from a hot wall to impinging water drops in the spherical state, Chem. Eng. Sci. 21 (1966) 1047–1056.
[29] A.L. Yarin, D.A. Weiss, Impact of drops on solid surfaces: self-similar capillary waves, and splashing as a new type of kinematic discontinuity, J. Fluid Mech. 283 (1995) 141–173.
[30] C. Mundo, M. Sommerfeld, C. Tropea, Droplet-wall collisions: experimental studies of the deformation and breakup process, Int. J. Multiphase Flow 21 (1995) 151–173.
[31] S. Toda, A study of mist cooling, Heat Transfer Jpn. Res. 1 (1974) 1–44.
[32] A.F.J. Baggerman, D. Schwarzbach, Solder-jetted eutectic PbSn bumps for flip-chip, IEEE Trans. Comp. Pack. Manuf. Tech. B 21 (4) (1998) 371–381.
[33] M. Rein, Phenomena of liquid drop impact on solid and liquid surfaces, Fluid Dyn. Res. 12 (1993) 61–93.
[34] Z. Zapryanov, S. Tabakova, Dynamics of bubbles, drops and rigid particles, Fluid Mechanics and its Applications, vol. 50, Kluwer Academic, Dordrecht, Boston, London, 1999.
[35] B. Kang, J. Waldvogel, D. Poulikakos, Remelting phenomena in the process of splat solidification, J. Mat. Sci. 30 (1995) 4912–4925.
[36] T. Bennett, D. Poulikakos, Heat transfer aspects of splat-quench solidification: modeling and experiment, J. Mat. Sci. 29 (1994) 2025–2039.
[37] W.E. Ranz, W.R. Marshall, Evaporation from drops I & II, Chem. Eng. Prog. 48 (1952) 173–180.
[38] S. Schiaffino, A.A. Sonin, On the theory for the arrest of an advancing molten contact line on a cold solid of the same material, Phys. Fluids 9 (1997) 2227–2233.
[39] S. Schiaffino, A.A. Sonin, Motion and arrest of a molten contact line on a cold surface: an experimental study, Phys. Fluids 9 (1997) 2217–2226.
[40] M. Pasandideh-Fard, R. Bhola, S. Chandra, J. Mostaghimi, Deposition of tin droplets on a steel plate: simulations and experiments, Int. J. Heat Mass Transfer 41 (1998) 2929–2945.
[41] T. Bennett, D. Poulikakos, Splat-quench solidification: estimating the maximum spreading of a droplet impacting a solid surface, J. Mat. Sci. 28 (1993) 963–970.
[42] S. Schiaffino, A.A. Sonin, Molten droplet deposition and solidification at low Weber numbers, Phys. Fluids 9 (1997) 3172–3187.
[43] D. Poulikakos, J.M. Waldvogel, Heat transfer and fluid dynamics in the process of spray deposition, in: Advances in Heat Transfer, vol. 28, Academic Press, 1996, pp. 1–69.
[44] J. Fukai, Z. Zhao, D. Poulikakos, C.M. Megaridis, O. Miyatake, Modeling of the deformation of a liquid droplet impinging upon a flat surface, Phys. Fluids A 5 (1993) 2588–2599.
[45] M. Pasandideh-Fard, J. Mostaghimi, On the spreading and solidification of molten particles in a plasma spray process: effect of thermal contact resistance, Plasma Chem. Plasma Process. 16 (1996) 83–98.
[46] D. Attinger, Z. Zhao, D. Poulikakos, Analytical estimation of the maximum spreading diameter during impact of a drop on a colder surface including thermocapillary and gravitational effects, in: ILASS, 1999.

[47] M.A. Carroll, M.E. Warwick, Surface tension of some Sn–Pb alloys: Part 1 Effect of Bi, Sb, P, Ag, and Cu on 60Sn–40Pb Solder, Mater. Sci. Technol. 3 (1987) 1040–1044.
[48] J.V. Naidich, Wettability of solids by liquid metals, Prog. Surf. Membr. Sci. 14 (1981) 353–484.
[49] J. Campbell, H. Conrad, Wetting kinetics of Molten 60Sn40Pb on a Ag–0.33 wt.% Pt thick film conductor, J. Electron. Pack. 117 (1995) 241–245.
[50] T.C.R. Company, CRC Handbook of Chemistry and Physics, 81 ed., CRC Press, Boca Raton, 2000.